Available online at www.sciencedirect.com

SciVerse ScienceDirect

Acta Materialia 60 (2012) 5370–5379

Acta MATERIALIA

www.elsevier.com/locate/actamat

Sample size matters for $Al_{88}Fe_7Gd_5$ metallic glass: Smaller is stronger

C.-C. Wang [a], J. Ding [b], Y.-Q. Cheng [b], J.-C. Wan [a], L. Tian [a,b], J. Sun [a], Z.-W. Shan [a,*], Ju Li [a,c,d,*], E. Ma [a,b,*]

[a] Center for Advancing Materials Performance from the Nanoscale (CAMP-Nano) & Hysitron Applied Research Center in China (HARCC), State Key Laboratory for Mechanical Behavior of Materials, Xi'an Jiaotong University, Xi'an 710049, China
[b] Department of Materials Science and Engineering, Johns Hopkins University, Baltimore, MD 21218, USA
[c] Department of Nuclear Science and Engineering, Massachusetts Institute of Technology, 77 Massachusetts Avenue, Cambridge, MA 02139, USA
[d] Department of Materials Science and Engineering, Massachusetts Institute of Technology, 77 Massachusetts Avenue, Cambridge, MA 02139, USA

Received 23 January 2012; received in revised form 6 June 2012; accepted 8 June 2012

Abstract

For metallic single crystals with dimensions in the micrometer and sub-micrometer regime, systematic studies have established that sample size has an obvious influence on the apparent strength, following a "smaller is stronger" trend. For amorphous metals, several metallic glasses (MG) appear to exhibit a similar trend, while a few others do not. Here, another MG is examined, $Al_{88}Fe_7Gd_5$, using quantitative in situ tensile and compression tests inside electron microscopes, with sample effective diameter covering a wide range (100 nm to 3 μm). A clearly elevated strength is observed, as high as about twice the value of bulk samples, for samples with diameters approaching 100 nm. A size regime is proposed, where the strength is controlled by the nucleation of the shear band, starting from its embryonic stage: the smaller the sample size, the more difficult this nucleation becomes. The size dependence is also discussed from an energy balance perspective: the resulting simple power law fits the data as well as other published strength data for a number of MG systems.

Keywords: Metallic glass; In situ TEM and SEM; Size effect; Strength; Tensile and compression

1. Introduction

Metallic glasses (MG) have been widely studied as a new class of advanced materials [1,2] owing to their desirable properties, such as outstanding yield strength and fracture strength, large elastic strain, and superior wear and corrosion resistance. At the same time, MG have advantages in net-shape thermoplastic molding and patterning when processed through the supercooled liquid regime [3]. A particularly interesting recent finding is that, at room temperature, these glassy materials can also turn quite malleable [4–8] and damage-tolerant [9–12], much more so when compared with their bulk counterparts, if their physical dimensions are on micrometer and especially sub-micrometer scales. Combining these attributes, a "the smaller the better" proposal has been put forward for MG [13]. As such, small-volume MG are especially attractive for applications such as in microelectromechanical systems.

It is of obvious interest to find out whether, and how, the strength of MG changes when their physical dimensions are small. For small-volume MG to find practical use, it would be desirable that their strength remained as high as, or even became elevated relative to, that of their bulk counterparts. Also, in terms of fundamental understanding of plasticity, the way in which the sample dimensions influence the strength of amorphous metals is an issue

* Corresponding authors. Address: Center for Advancing Materials Performance from the Nanoscale (CAMP-Nano) & Hysitron Applied Research Center in China (HARCC), State Key Laboratory for Mechanical Behavior of Materials, Xi'an Jiaotong University, Xi'an 710049, China (Z.-W. Shan, J. Li, E. Ma).

E-mail addresses: zwshan@mail.xjtu.edu.cn (Z.-W. Shan), liju@mit.edu (J. Li), ema@jhu.edu (E. Ma).

1359-6454/$36.00
http://dx.doi.org/10.1016/j.actamat.2012.06.019

of scientific importance. For crystalline materials, the effects of sample size on apparent strength have received much attention recently [14,15]. For single-crystal metals in the micrometer and submicron regime, a "smaller is stronger" trend has been established, because the smaller the sample size, the more difficult the nucleation and operation of dislocations become, elevating the stresses required to cause yielding and sustain plastic flow [14–18]. However, these findings cannot be directly extrapolated to MG, because the MG have an amorphous internal structure and no dislocations to speak of. It is therefore intriguing whether a parallel/analogous "size effect" can also exist for the MG strength.

A number of experiments have already been carried out in recent years to look into the possibility that sample size influences the apparent strength of MG. A variety of alloy systems have been examined, including MG based on Pd [5,19], Zr [6,11,20–26], Fe [26] and Mg [26,27]. Unfortunately, the results have led to a controversial debate. Several groups reported that there is size-strengthening when the MG dimensions are reduced into the micrometer and sub-micrometer regime [6,20,21,24,26,27], while others claim little or no size dependence of the apparent strength [10,11,19,25,28].

The present work addresses this question in another MG system, $Al_{88}Fe_7Gd_5$, with sample sizes covering a wide range (effective diameter from 100 nm to 3 μm). The strength is measured using quantitative in situ testing: compression tests in both transmission electron microscopy (TEM) and scanning electron microscopy (SEM), and tensile tests inside a TEM instrument. The combined data sets are found to indicate a "smaller is stronger" trend. In particular, a clearly elevated strength to about twice that of bulk samples has been observed for this MG with diameters approaching 100 nm. All the $Al_{88}Fe_7Gd_5$ samples for which the strength is controlled by shear band formation are grouped together, and their size-dependent strength is modeled by extending/modifying previous ideas based on energy balance considerations [5,10,15,29]. The derived power-law size dependence also fits well to other published strength data for a number of MG systems that appear to exhibit sample size dependence, collapsing all data onto a single plot. Three size regimes are proposed, in term of different sample size dependence of strength.

2. Experimental details

$Al_{88}Fe_7Gd_5$ MG ribbons with nominal thickness ~50 μm were produced by melt spinning. Ribbons 3 × 3 mm square were cut and mechanically and chemically polished on both sides to <20 μm. On these slices, a set of micrometer-sized or submicron-sized beams (or pillars) with effective diameter D were fabricated via micromachining, using a Helios NanoLab 600i dual-beam focused ion beam (FIB) system. In order to minimize the potential ion irradiation effect, the final step of FIB fine milling was performed under a lowered voltage (15 kV) and current (16 pA). For compression tests, pillars with size D (at half height of pillars) ranging from 100 nm to 3 μm (aspect ratio 3~4) were fabricated. In situ compression tests were conducted inside the chamber of both the FIB system ($D = 500$ nm to 3 μm) and a JEOL JEM-2100F TEM instrument ($D = 200$–900 nm), employing a Hysitron PI85 SEM PicoIndenter and a Hysitron PI95 TEM PicoIndenter, respectively. Both these instruments were able to acquire the force–displacement data with resolution less than ~0.4 μN and ~1 nm and simultaneously monitor the deformation processes [9], which were recorded by the digital CCD camera equipped with a SEM or TEM system. For tensile samples, to minimize the sample thickness difference during the final top-down thinning of tensile specimens, the sample stage was tilted ±1.8° relative to the ion beam direction [30]. The nominal diameter for the tension specimen is defined as $D = A^{1/2}$, where A is the cross-sectional area. Tensile testing of beams with size D ranging from 100 to 400 nm and aspect ratio 4~8 was carried out in situ by TEM using a Hysitron PI95 TEM PicoIndenter. For tension testing, a tungsten grip was fabricated using FIB [30]. For pillar compression, a flat diamond punch was used. All tests were carried out with a strain rate of 2.0×10^{-3}–2.0×10^{-2} s^{-1}.

3. Results

Based on the testing methods and their physical size, the samples were classified into four groups, as outlined in Table 1.

3.1. Compression tests

Shear banding appears to be the dominant plasticity mode for group I samples. One typical example is shown in Fig. 1. Fig. 1a–c displays the SEM micrographs from a displacement-controlled compression test in the chamber of the FIB system (extracted from the recorded Movie 1 in online supporting materials), showing the plastic deformation of a typical $Al_{88}Fe_7Gd_5$ MG pillar with diameter $D = 2523$ nm. Fig. 1d is the corresponding engineering stress–strain curve. A shear band initiated from the side wall and running across the entire pillar (hereafter referred to as the mature shear band) can be seen clearly, as indicated by the white arrow in Fig. 1b. Correspondingly, a precipitous stress drop is observed in Fig. 1d. This is because the shear banding produces a displacement rate beyond that set by the program; the load cell responds by quickly dropping the force applied. Further loading led to the sudden collapse failure of the tested sample (Fig. 1c). The shear banding and failure process occurred so fast that the feedback control system could not respond in time. As a consequence, significant displacement bursts are observed in the displacement vs. time curve (inset in Fig. 1d).

It is known from earlier work on MG [6,20] that the influence of sample size on strength, if it exists, would be

Table 1
Classification of the tested samples.

Samples	Compression		Tensile	Size range (nm)	Deformation morphology
	SEM	TEM	TEM		
Group I	Y	–	–	900–3000	Shear band dominant
Group II	Y	Y	–	300–900	Mushroom and mature shear band
Group III	Y	Y	–	170–300	Mushroom without mature shear band
Group IV	–	–	Y	100–400	Shear band

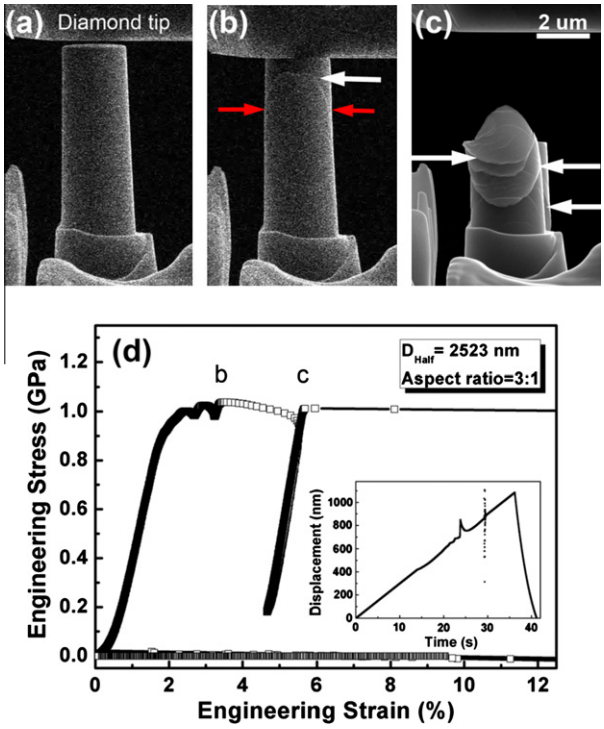

Fig. 1. A typical in situ microcompression test of $Al_{88}Fe_7Gd_5$ MG pillar with diameter 2523 nm in SEM. (a) and (b) are SEM micrographs extracted from a digital image stream. The original pillar (aspect ratio 3:1) has a taper ~1°. (b) Formation of a shear band passing through the pillar; the white arrow marks the formed shear band. (c) A still SEM image of the pillar after a large strain burst; several shear bands are formed. (d) The corresponding engineering stress–strain curve (the stress is defined as load divided by cross-sectional area at half height of pillar), with the inset showing the displacement-controlled loading function (strain rate $\sim 4 \times 10^{-3}\,s^{-1}$). The red arrows show the method of defining and measuring the diameter for strength calculation during the initiation of shear band. (For interpretation of the references to colour in this figure legend, the reader is referred to the web version of this article.)

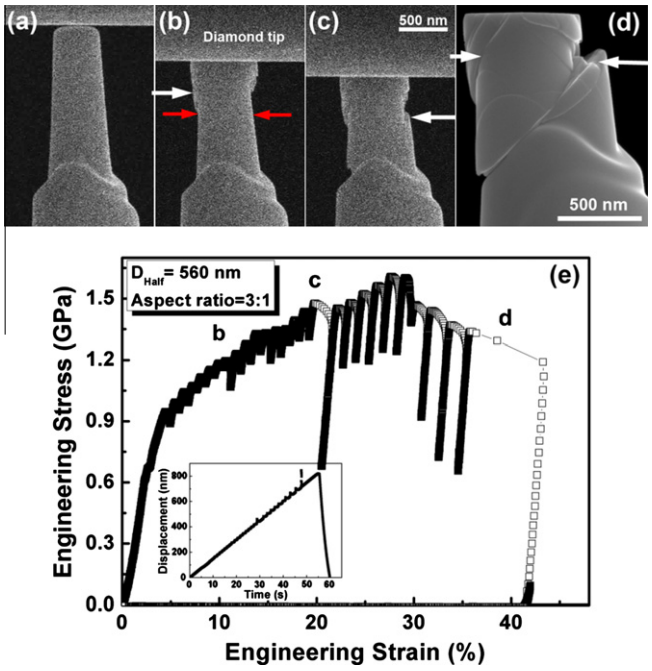

Fig. 2. An in situ compression test of $Al_{88}Fe_7Gd_5$ MG pillar with diameter 560 nm in SEM. (a) The original pillar (aspect ratio 3:1) has a taper ~2.5°. (b) The plastic deformation through small shear offsets localizes at the top of the pillar, forming a "mushroom-like" morphology. (c) A larger shear offset forms along a ~41° plane with respect to the loading axis. (d) A still SEM image of the pillar after testing, the white arrows show the shear bands. (e) The corresponding engineering stress–strain curve (strain rate $\sim 8 \times 10^{-3}\,s^{-1}$). The red arrows show the diameter measurement for strength calculation during initiation of shear band. (For interpretation of the references to colour in this figure legend, the reader is referred to the web version of this article.)

expected to become increasingly more pronounced as D decreases into the lower sub-micrometer range. This is analogous to the published D^{-m} dependence for crystals (for face-centered cubic metals, for example, $m \approx 0.6$) [15,17]. The compression test was therefore also extended to group II samples. This group of samples is small enough that they can be tested in situ in the TEM, as the forces required are now within the limit of the Hysitron PI95 PicoIndenter load cell.

Unlike group I samples, mushroom-like sample morphology begins to develop during deformation prior to the formation of the first major shear band for group II samples, regardless of whether the samples are tested in the SEM or TEM. Presumably, this is mainly due to the increasing stress gradient stemmed from the taper geometry with the decrease in sample diameter [31]. One typical example is shown in Fig. 2. The pillar had a smaller diameter, $D = 560$ nm. SEM images in Fig. 2a–d (corresponding to that marked in Fig. 2e) display the morphology evolution under compression (also see Movie 2 in online supporting material). A mushroom-like geometry formed at the free end of the sample (Fig. 2b) prior to the set in of the first major stress drop (Fig. 2e). Further loading led to the formation of multiple shear bands (Fig. 2d) and the significant serrations in the stress vs. strain curve (Fig. 2e).

The localized deformation or mushroom-like deformation geometry are very probably the artifacts resulting from the taper geometry as well the potential imperfect contact (e.g. misalignment, surface asperity) between the flat punch diamond probe and the sample. Both factors play an

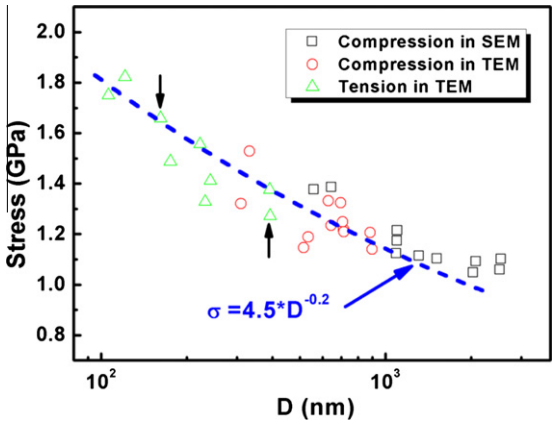

Fig. 3. Strength vs. sample diameter (D) of the $Al_{88}Fe_7Gd_5$ MG. For the tension group, fracture strength is used because all tensile samples fracture upon shear banding. For the compression group, the strength corresponds to the yield strength for the initiation of mature shear band in pillars. The two points marked by black arrows are for samples under e-beam-off tensile tests.

increasing role with the decrease in sample diameter. In order to characterize the intrinsic properties of as-studied samples accurately and precisely, the strength of the samples is defined as the formation stress of the first mature shear band, i.e. a shear band initiating from the side wall and running across the entire sample (Figs. 1b and 2c). The formation of such shear bands inevitably led to a major stress drop in the stress–strain curves (e.g. Figs. 1d and 2e). In addition, the instantaneous diameter measured at the initiation site of the first mature shear band (as indicated by the red arrows in Figs. 1b and 2c) is used to calculate the strength as defined above instead of using that read directly from the engineering stress–strain curve.

The strengths for the group I and II samples are plotted as functions of D in Fig. 3, using open squares (tested inside the SEM) and open circles (tested inside the TEM), respectively. A general trend of these data points is that they are higher than the bulk strength (~1.0 GPa, of the order of $0.02E$, where E is the Young's modulus of this MG) [32,33]. For samples with diameter <900 nm or so, an obvious size dependence, i.e. smaller is stronger, is observed. The measured strengths of group II samples from SEM and TEM testing are comparable; this overlap suggests that the transition trends seen from these two groups could not come from different testing machines, but are more likely due to sample size effects.

With decreasing D (group III), "homogeneous-like" plastic flow becomes dominant for the compression test. One typical example is shown in Fig. 4. Dark-field TEM images for the $D = 226$ nm sample before and after testing are shown in Fig. 4a–d, with corresponding engineering stress–strain curve in Fig. 4e. These figures (in Movie 3 in online supporting materials) show that stress drops associated with major shear are no longer obvious. Instead, some distributed deformation changed the sample shape from the initial 3.5° taper to become almost taper-free

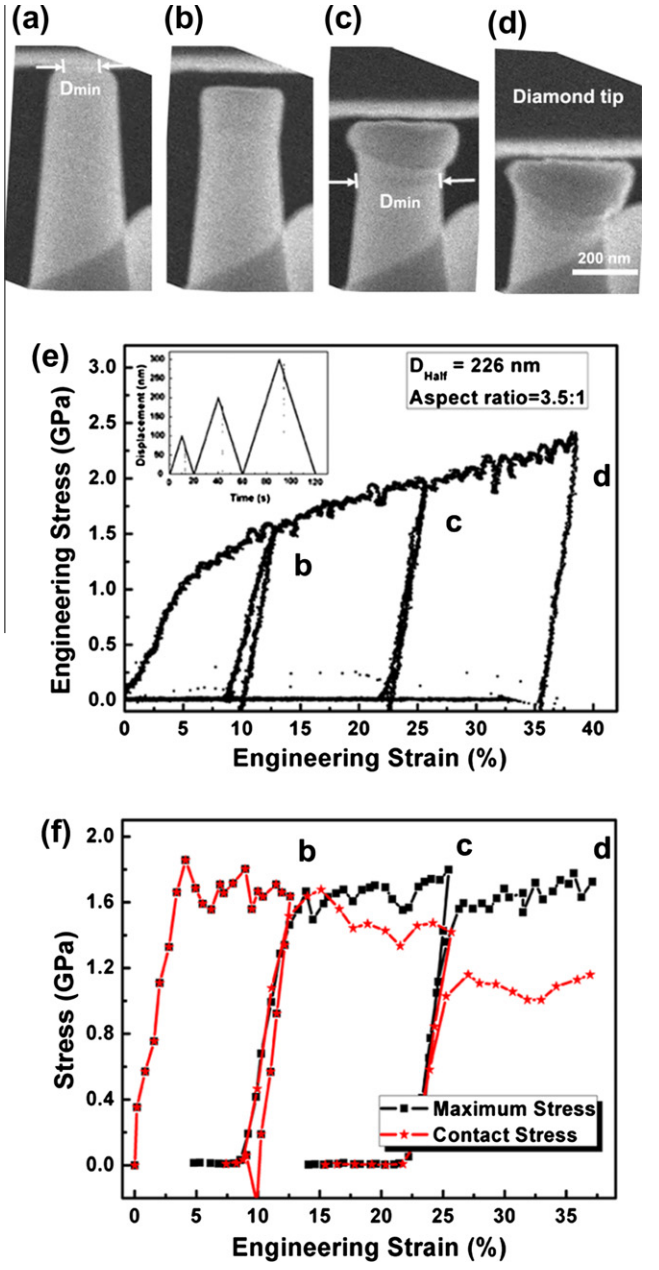

Fig. 4. In situ nanocompression of $Al_{88}Fe_7Gd_5$ MG pillars with $D = 226$ nm inside a TEM. (a)–(d) are dark-field TEM images showing the evolution during the three consecutive loading–unloading tests. The original pillar with a taper 3.5° becomes almost taper-free after the first loading in (b). (e) The corresponding engineering stress–strain curve (loading function in inset) with a strain rate $\sim 10^{-2}$ s^{-1}. (f) The contact stress vs. strain and maximum stress vs. strain curves, calculated based on the measured contact diameter and minimum diameter, respectively. The maximum stress shows a plateaued stress after 5% strain, while the contact stress gradually decreases owing to softening in the plastically flowing glass.

(Fig. 4b) after the first compression (corresponding to "b" in Fig. 4e). After unloading, the subsequent (second and third) loading moved the plastic deformation front forward, while the top part of the pillar changed to a "mushroom-like" morphology, as shown in Fig. 4c and d, corresponding to "c" and "d" in Fig. 4e. During this

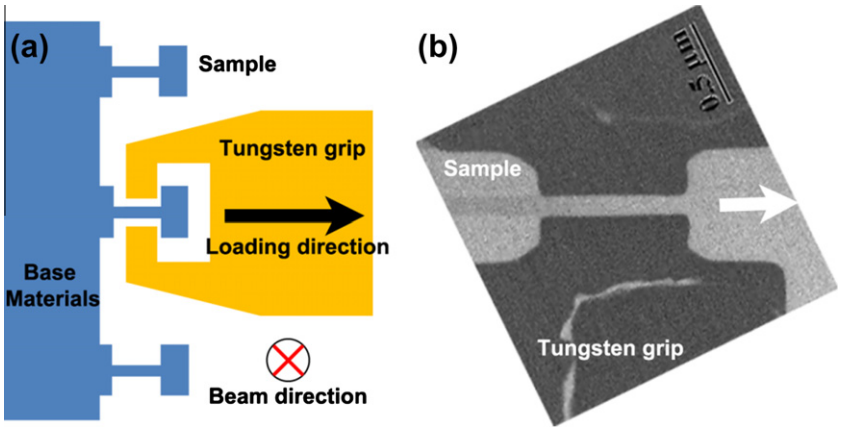

Fig. 5. (a) Schematic experiment setup for in situ nanotension test inside a TEM. (b) A centered dark-field TEM image of the sample-tungsten grip assembly. Arrows show the loading direction.

stage, some minor localized shear (or mild shear banding) may also have occurred, which could be detected from the sample morphology in the TEM images (Fig. 4c and d) and movies. But again, such localized deformation becomes less obvious with decreasing D, which is consistent with the recent report that Al-based MG has a relatively large brittle-to-ductile transition size of ~300 nm [28].

The evolution of the area of the contact interface between the pressing punch and the sample was monitored in situ by directly measuring the changing diameter from TEM images. This allowed the true contact stress (load divided by instantaneous contact area) to be plotted as a function of engineering strain, as shown in Fig. 4f (red curve). This stress is seen to decrease gradually after yielding (more discussion on this stress evolution is presented in Section 4.2); the smallest cross-sectional area in the pillars was also measured, such that the maximum stress withstood by the pillar could be calculated along with straining. This stress stayed at almost a constant level after yielding, without "work hardening", as shown in Fig. 4f (black curve).

In this group III size regime, the yield strength exhibits a more apparent increasing trend. For example, the yield strength of the $D = 226$ nm pillar (~1.7 GPa) is ~54% larger than that of the $D = 2523$ nm pillar (~1.1 GPa). The corresponding elastic strain limit was estimated from the unloading curve in Fig. 4f to be 3.2%.

However, although group III data suggest marked size strengthening, the plastic deformation results from considerable "homogeneous-like" flow, and shear banding has become mild and unobvious from the stress–strain curve and the images. In fact, as shown in Fig. 4, the top of the pillar experienced apparent softening, leading to a mushroom shape (see Section 4.2 for discussions on flow stress). Such a mixed mode of plasticity was reported before for small MG samples [5,10,11,19]. This makes it questionable whether one can directly compare the strength of these samples with those larger samples in group I and group III, for which shear banding is the dominating mechanism. In Section 3.2, additional experiments allowed comparison of the strength values controlled by shear banding only. For the small sizes in the group III regime, shear banding turned out to remain dominant in tensile experiments.

3.2. Tensile tests

While mixed mechanisms rule the compression tests of group II and especially group III sizes, it will be shown next that shear banding remains the dominant mode (and probably the sole mode) of plastic deformation in the tensile case, even for very small samples with $D = 100$–400 nm. These tensile samples, tested inside the TEM, will be designated as group IV. Fig. 5a shows a schematic of the experiment setup for the tensile test inside the TEM, and Fig. 5b displays a centered dark-field TEM image of the actual tungsten grip–sample assembly. In order to ensure intimate sample/grip contact at the interface, three consecutive loading–unloading runs were conducted for a given sample. After a careful measurement of the sample cross-sectional area from a postmortem SEM image (e.g. inset in Fig. 6a), and of the elongation of the beam from the still frames (Fig. 6b–e), the calibrated stress–strain curve was obtained from the recorded load–displacement data. Fig. 6a gives the curve for the $D = 106$ nm sample as an example. The overlap of loading and unloading curves indicates that the beam (gauge length) experienced only elastic deformation. Fig. 6b–f shows the TEM snapshots extracted from the recorded movie, corresponding to various instants during the three loading–unloading cycles in Fig. 6a. The first loading elongated the gauge length elastically by 1.9%, and the second loading to 3.9%. Upon the third loading to about the same strain, shear band set in as the only mode of plastic deformation, and fracture immediately ensued (see Movie 4 in online supporting materials). The corresponding strength is ~1.75 GPa, considerably higher than bulk Al-based MG samples (0.6–1 GPa in compression) [32,33]. The fracture occurred along a ~59° plane with respect to the loading axis, consistent with the previously reported cases for tensile failure in bulk MG (~48–60°) [2].

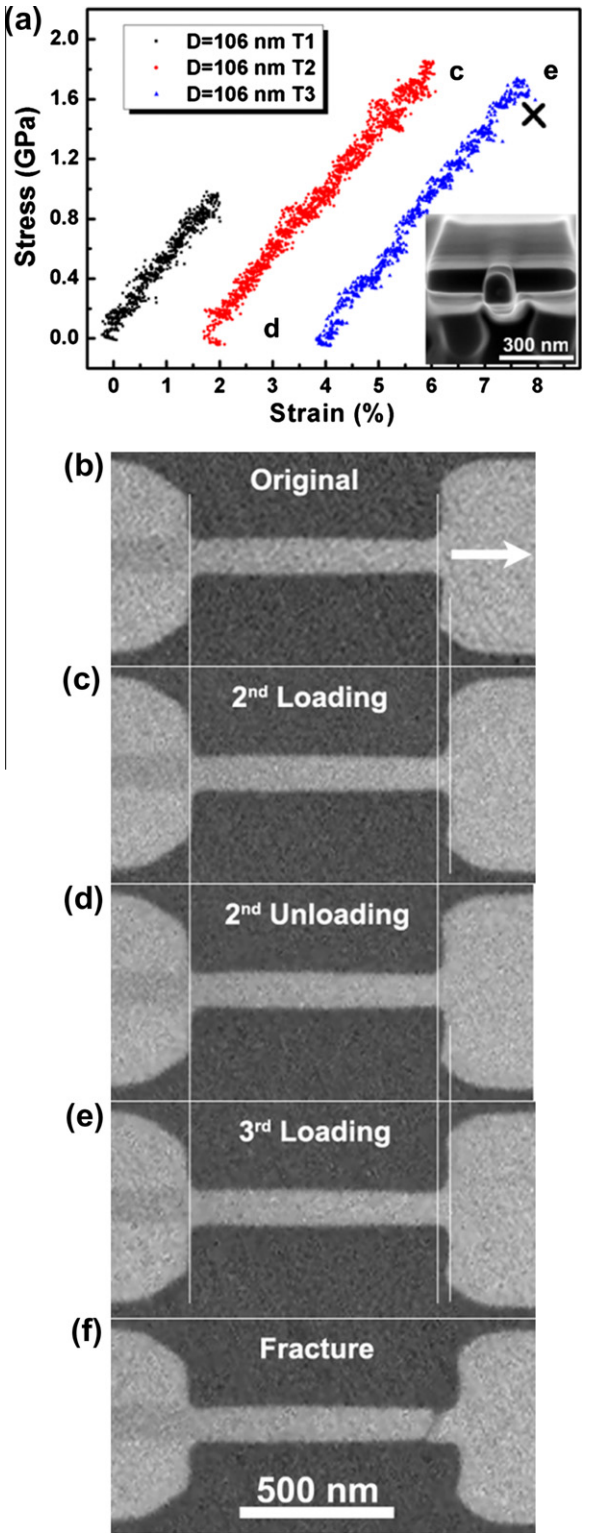

Fig. 6. In situ tension test of the $D = 106$ nm sized $Al_{88}Fe_7Gd_5$ MG beam (aspect ratio = 7.5:1) inside a TEM. (a) The tensile engineering stress–strain curve of the beam under a strain rate$\sim 6 \times 10^{-3}$ s^{-1}; the three loading–unloading runs are shifted for clarity. Inset shows the SEM micrograph of the cross section of the fractured beam, from which the stress is calculated. The strain is calibrated using the still frames extracted from a recorded movie, as shown in (b)–(f). The beam is elastically strained to 3.9% before shear banding and fracture.

All the group IV samples exhibited elastic deformation, followed by fracture along with the onset of shear banding. The measured E, from the tensile stress–strain curves, is $\sim 45 \pm 5$ GPa, close to the bulk value (Young's modulus $E \approx 50$ GPa) [33]. There was no obvious homogenous-like flow or necking (at least at the present strain rates), which would otherwise complicate the stress evaluation and comparison (complex multi-axial stress in the neck) [4,6]. The tensile strength data of group IV samples are added to Fig. 3 (open triangles). These data are consistent with the trend seen from other samples, and corroborate the "smaller is stronger" trend. Along with the increased strength, the elastic strain achieved also increased with decreasing D (106 nm/3.8%, 121 nm/3.9%, 175 nm/3.3%, 222 nm/3.2%, 232 nm/3.3%, 242 nm/3.0% and 391 nm/2.9%), as measured from TEM images. The tensile strength and elastic strain limit are about twice those of bulk samples of Al-based MG ($\sim$1.0 GPa and $\sim$2%) [32]. It is therefore concluded that small samples indeed exhibit a strong size effect. In other words, sample dimensions influence the apparent strength to such an extent that the tensile strength can be doubled for $\sim$100 nm samples relative to bulk samples.

For samples as small as $D \approx 100$ nm, the electron beam effect becomes a concern, since the in situ tests were conducted under e-beam illumination inside the electron microscope. This "beam effect" possibility has been excluded through two additional tests of samples with sizes in the group IV regime. For tensile testing $D = 162$ nm and $D = 393$ nm samples under beam-off conditions (the e-beam was blocked off such that only mechanical data were taken, with imaging only after the test [34]), no obvious change in strength and deformation mode was observed compared with the beam-on situation. These two data points have also been included in Fig. 3 (marked by black arrows). Note that any e-beam enhanced surface diffusion or heating would decrease the apparent strength. Therefore, the elevated strength observed for group IV (and group II and III as well) samples relative to larger and bulk samples cannot be attributed to e-beam effects. Three additional samples in the tensile data set exhibited strength obviously lower than the rest; inspection of the load–time and displacement–time records during loading found obvious glitches, which could arise from grip/sample contact asperities or sample imperfections. In addition, these appear to be indications of misalignment. These three points are therefore not included in Fig. 3.

4. Discussion

4.1. Compression vs. tensile tests

Obtaining reliable mechanical property data for nanoscale samples is a non-trivial proposition. Indeed, a major source of controversy regarding the size effect in MG is likely to stem from testing difficulties and inconsistencies. As an example, the small testing volume may be subject

to variations in the content, size and distribution of defects and, together with the delicate manipulation of tiny samples in the testing devices, often renders large scatter in data. Some authors have thus concluded that "smaller is more stochastic" [23].

Another origin of artifacts arises from the scheme of micropillar/nanopillar compression test itself, which has been widely employed in the vast majority of previous experiments on small MG samples [5,9,10,15,19,22,27,35,36]. The compression test data often show quite some scatter and, as this paper has illustrated, relatively small compression samples involved to a great extent additional plastic flow mechanisms other than shear banding. These observations are known for other MG as well, reported earlier by other groups [11,19,23], making the measured strength comparison less conclusive. In general, the approach of compression of micropillars or nanopillars suffers from a number of inherent problems, e.g. promotion of localized deformation in tapered pillar with rounded top [19], buckling or bending of pillars with large aspect ratio [10,20,35], contact interface serving as sites for heterogeneous nucleation of shear bands [22], and friction and confinement at the contact area between punch and pillar. All of these would contribute to data scatter and uncertainty.

Compared with compression, tensile testing is a more standard and informative method of revealing fundamental deformation properties. A quantitative tensile test of several submicron MG was performed inside a SEM earlier, and the data do suggest a sample size dependence of strength [6]. The TEM tensile approach not only alleviates many of the problems mentioned above, but also offers much better spatial resolution (than SEM), which improves the challenging alignment for tiny samples, measures the elongation more accurately and monitors continuously along deformation the internal structural evolution in the glass. The tensile data reported in Fig. 3 are therefore more conclusive that small sample dimensions do influence the apparent strength of MG. Also, the group IV tensile samples retained shear banding as the controlling plasticity mechanism (possible reasons are discussed in Section 4.2), making it more justifiable to compare the strengths measured in the $D = 100$–400 nm regime with larger samples up to the bulk regime, to establish the general "small is stronger" trend over a wide size range.

Some sample sizes have both compressive strength and tensile strength (Fig. 3). In general, the compressive strength may be expected to be slightly higher than the tensile strength according to the Mohr–Coulomb criterion presumably applicable to MG [2]. In the current data collection, the scatter of the data points, the mixed plasticity mode in compression-tested group II samples and the different sample aspect ratio used for the tensile and compression samples make it difficult to conclude on the tension–compression asymmetry. All one can say is that the tensile and compressive data are comparable in revealing a similar trend.

4.2. The origin of the sample size effect on MG strength

The results above have shown an appreciable sample size dependence of strength for MG in the micron to submicron size regime. The presence of such a sample size effect on the apparent strength of MG may be a bit surprising, considering that there are no line defects such as dislocations in crystals, whose operation could sense the presence of "boundary conditions" (e.g. owing to the constraining surfaces in smaller pillars, an operating Frank–Read source would be expected to have a shorter length and a larger curvature for the bowing segment) [15].

The present paper proposes, using a schematic diagram (Fig. 7), the expected trend for the apparent strength of a MG sample as a function of its physical size. In Regime I (sample sizes from a few microns to bulk scale), because of the inevitable presence of some minor extrinsic flaws and a wide distribution of inherent structural defects (such as liquid-like regions [37]) in the MG internal structure, there are always potent preferential sites that make shear band initiation very easy. As a result, the generation of embryonic shear bands is not the strength-controlling process. The observed yield strength ($\sim 0.02E$) for bulk MG [38] thus corresponds to the flow stress, σ_f, which is the stress required to maintain the spreading or sliding of an already-nucleated shear band. In other words, the strength in this case corresponds to the stress needed to sustain high-rate shear in shear band propagation [39]. σ_f/E is always ~ 0.02 and almost independent of the way in which the MG is prepared [39]. In this regime, the apparent strength is insensitive to sample size, which is observed in experiments of bulk MG samples [40,41].

When sample size decreases into the micron or submicron regime, Regime II in Fig. 7, there would be negligible extrinsic flaws (at least not observable under TEM), and the defects in the glass structure (and their groups) become small in size and low in population, such that shear band initiation becomes an issue. Shear banding thus becomes "nucleation controlled" at the outset of its formation.

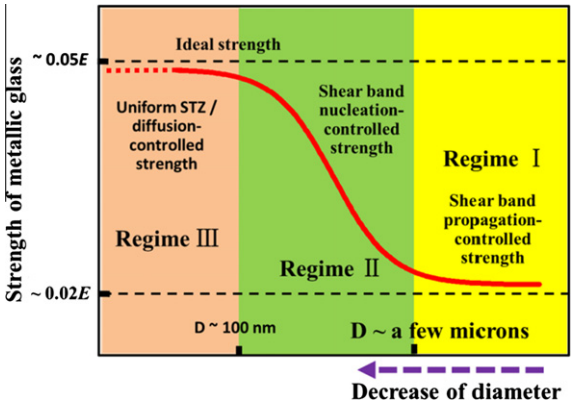

Fig. 7. Schematic showing the proposed general trends for the size-dependent strength of MG, with three regimes corresponding to different strength-controlling mechanisms.

The strength then corresponds to the stress needed for initiating shear banding from its embryonic stage. The latter, the present authors stipulate, is dependent on sample size. This size dependence can be understood from the following atomic-scale viewpoint. Upon loading, the shear transformations that carry plastic events in MG will initially operate stochastically, independent of each other from fertile sites (shear transformation zones, STZ) in the glassy structure, but they gradually gain correlation both temporally and spatially, and self-organize into a larger and larger flow zone [42]. The larger these collective flow defects (e.g. high aspect ratio of the STZ percolation/collection), the higher the stress concentration, and the greater the possibility for them to reach the threshold that would trigger the self-sustaining shear banding [9]. In a sample with very small (e.g., submicron-sized) volume, STZ and their groups may instead self-organize into a network, with less chance for percolation into a shear band. This is analogous to the percolation of dislocations in crystals [17,43], which is also sample size dependent. As such, the smaller the sample, the higher stress it requires to generate a shear band at a fixed strain rate. Decreasing the sample size in Regime II therefore drives up the stress σ_I needed for initiating a shear band towards the ideal strength of MG, the predicted $\sim 0.05E$ [39,41].

One eventually arrives at Regime III (Fig. 7) when one reaches the strength ceiling, i.e. the highest stress that can be reached when shear band initiation is the most difficult. With further reduction of size, shear banding becomes so unfavorable that it subsides altogether and gives way to STZ operations everywhere, to plastically flow the sample in a "homogeneous-like" fashion. However, for such tiny samples, surface diffusion or other flow mechanisms could come into play and become gradually dominant with decreasing strain rate [18], possibly giving rise yet again to a size dependence, such as a decreasing strength relative to the flat dashed line postulated in Fig. 7.

The spread-out STZ actions, i.e. some "homogeneous-like" plastic flow, are more obvious under the confinements imposed in the compression test mode, owing to the tapered and rounded geometry, friction between the punch and the pillar, and multi-axial stress state. As indicated in Fig. 4 and also earlier findings [5,9–11,44], plasticity in this case is being gradually initiated in the form of mild shear bands and increasing homogeneous-like flow with decreasing size. Since $\sigma_f < \sigma_I$, the overall stress is gradually decreasing in the stress–strain curve (Fig. 4f), as more and more regions of the pillar are driven into the flow state. The initial yield strength (the open circles in Fig. 3) may be close to σ_I, but the ensuing plastic deformation consists of already initiated flow (requiring σ_f) as well as the spreading of shear in other regions. Eventually, the entire top part of the pillar is flowing, approaching σ_f.

In contrast, under uniaxial tension, the tensile stresses would facilitate cavitation in flowing shear bands. Previous studies have revealed that, in an Al–Fe–Gd MG, the tensile-deformed region tends to contain nanovoids much more so than compression-deformed regions [45] (cavities in shear band should close if always under local compression). As such, fast failure is expected once the shear band forms, even if a small one, leaving little chance for appreciable "homogeneous-like" plastic flow to come in and carry plastic flow. This is a likely reason for the obvious difference between group III (compression) and group IV (tension) samples in the $D = 100$–400 nm regime. Even though substantial homogenous-like deformation (minor shear and STZ-mediated activities) was observed in the compression samples, shear banding remained the predominant plastic deformation mode in group IV tensile samples, as shown in Fig. 6.

4.3. Size dependence of MG strength: a semi-quantitative power-law representation

Size dependence of the strength, specifically the "smaller is stronger" trend, was proposed in Section 4.2 (Regime II in Fig. 7). However, quantitative and physical modeling of this behavior would require detailed knowledge of shear band dynamics regarding the transition from propagation controlled mode to nucleation controlled mode. In the latter case, for example, the strength would be determined by the way in which the STZ organize themselves prior to and during the deformation, changing their behavior with and without the presence of surfaces. Such a level of understanding is unfortunately not yet available, despite recent progress in understanding shear band dynamics on both simulation [29,39,41] and experiment [46,47] fronts.

In the interim, to facilitate a quantitative representation of experimental data, the present authors take a broad-stroke approach and follow the spirit of previous energy-balance models. The energy cost per unit area of the shear band created is assumed to be a constant Γ, regardless of the sample size. The size effect is then borne out of dimensional origin (i.e. three-dimensional energy source vs. two-dimensional energy sink). Such a simplified route was first adopted by Volkert et al. [5], which was followed in several later studies [6,8,25,48,49]. Specifically, they treat the shear band like a crack driven by the release of all the stored elastic energy in the sample body. Assuming relations analogous to the Griffith's crack equation, the driving stress was derived to be

$$\sigma = \sqrt{2^{3/2}\Gamma E/H} \tag{1}$$

where H is the height of the sample (proportional to D for the given aspect ratio used in a test). Eq. (1) predicts a $D^{-0.5}$ power-law dependence for the strength [5,6]. At large samples sizes, Eq. (1) predicts that the strength would diminish to zero, while in reality the strength limits to a relatively high bulk strength value on the GPa level. Also, Eq. (1) does not appear to quantitatively fit the experiment data by several groups [5,6,25]. Plotting the strength data directly vs. D for group I, II and group IV samples, a fitting exponent of $m = 0.2$ was found

for the D^{-m} dependence in Fig. 3, again inconsistent with the model in Eq. (1).

The model in Eq. (1) was modified later by several authors [15,29]. In these developments, the stress drop in the stress–strain curve is assumed to correspond to shear banding, and the elastic energy released in the particular stress drop is used to drive the shear band. This idea will be extended below, to arrive at a new power-law description of the size dependence of strength.

It is assumed that the measured strength is governed by the stress σ_I needed to initiate a single shear band. A main shear band can be the cause for the onset of plastic deformation in sub-micron or micron-sized MG (e.g. in group I, II and IV samples). After shear band initiation, the stress required becomes the flow stress σ_f, which maintains the propagation/sliding of shear band. Assuming adiabatic conditions, the released elastic energy from the sample volume due to the elastic strain energy difference is equal to the energy consumed by shear band formation:

$$\left(\frac{\sigma_I^2(D)}{2E}-\frac{\sigma_f^2}{2E}\right)\frac{(D^2\pi)H}{4}=\sqrt{2}\frac{D^2\pi}{4}\Gamma \tag{2}$$

The resulting size effect of strength is then

$$\sigma_I^2(D)-\sigma_f^2=2\sqrt{2}E\frac{\Gamma}{H}=2\sqrt{2}E\frac{\Gamma}{aD}=\frac{\Psi}{D} \tag{3}$$

where $a=\frac{H}{D}$ is the sample aspect ratio and $\Psi=2\sqrt{2}E\frac{\Gamma}{a}$ is constant for a particular MG and a. As illustrated before [39], σ_f is the resistance against localized severe shearing associated with shear band itself. For a given MG, σ_f does not change significantly for various sample preparation conditions and can be deemed independent of sample size, whereas σ_I is sensitive to flaws and glass structure and hence strongly dependent on the way in which the MG is made. In the present discussion, σ_I is also a function of sample size D.For bulk samples of MG, D is large and $\frac{\Psi}{D}\to 0$, such that the observed strength approaches σ_f, with $\sigma_f=\sigma_o$, where σ_o is the bulk strength (the plateau in Regime I in Fig. 7). Plugging this into Eq. (3), one arrives at

$$\sigma_I^2(D)-\sigma_o^2=\frac{\Psi}{D} \tag{4}$$

Although this line of reasoning is a crude approximation and does not unravel the detailed mechanisms underlying Regime II in Fig. 7, the limiting case of Eq. (4) serves the purpose of providing one functional form (the present authors call it "shifted-$D^{-0.5}$") to semi-quantitatively represent the size dependence. Fig. 8 presents a double-log plot based on Eq. (4), for the strength of $Al_{88}Fe_7Gd_5$ MG vs. D. Included here are only the samples for which the strength is controlled by shear banding, satisfying the premise of the model leading to Eq. (4). Fig. 8 also includes the available experimental data for four other different MG. The slopes of the linear fits indeed approach unity, as predicted by Eq. (4). The intercept on the vertical axis gives Ψ, which depends on the Young's modulus, sample aspect ratio and energy per unit area of shear band (the latter is unknown) of different MG systems. This fitting parameter also absorbs other uncertainties and scaling factors.

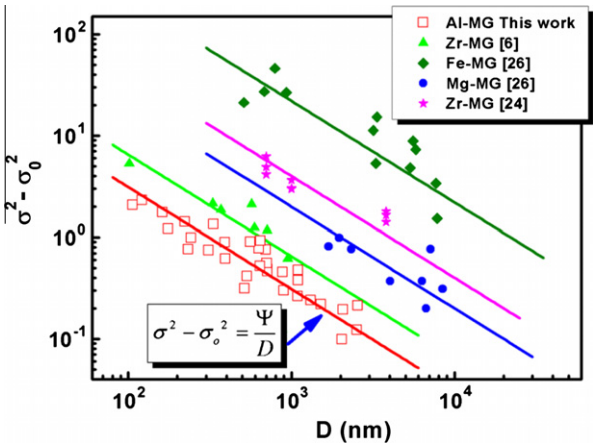

Fig. 8. Linear fit based on $\sigma^2-\sigma_0^2\sim\frac{\Psi}{D}$ of the size-dependent strength of Al-based MG data and other four MGs at micrometer- and submicron-scale (in a double-log plot). The intercept of the y axis is $\lg\Psi$, which depends on the Young's modulus, aspect ratio and energy per unit area of shear band of MG systems.

Fig. 9 summarizes all the published data in another format, except two cases that do not seem to exhibit any size dependence [10,28]. All these data collapse onto a single curve in this plot. There appears to be a universal shifted-$D^{-0.5}$ power-law dependence of strength with decreasing diameter, with Eq. (4) serving as a semi-quantitative description.

Previous studies have already noticed that the magnitude of stress/load drops (corresponding to shear banding) in experimentally measured stress–strain curves (or load–displacement curves) from pillar compression depends on sample size [10,36]. When the shear band glides drastically over a long distance (large shear offset), a complete load drop (to zero stress) results. For moderate shear in smaller pillars, which are slower in time and shorter in distance, the feedback system responds fast enough for the pressing

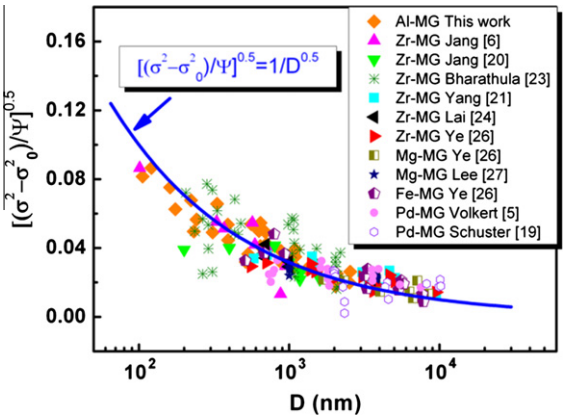

Fig. 9. A general model (based on shear band initiation) is used to fit the experiment data and other published data for size-dependent strength in various MG at the micro- and nanoscale, giving a shifted-$D^{-0.5}$ dependence. The literature strength data used in this plot are all for samples that exhibited shear banding as the controlling mode for yielding.

punch to quickly regain contact with the sample. The measured magnitude of load drop on the curves therefore only indicates the transient load response due to shear banding in a non-equilibrium state, and cannot be directly correlated with the intrinsic flow stress for shear band propagation.

5. Summary

In summary, through in situ tensile and compression testing of $Al_{88}Fe_7Gd_5$ MG with a wide range of effective diameters ($D = 100$ nm to 3 μm) inside the TEM and SEM, a clear "smaller is stronger" trend was observed. In particular, in submicron-sized samples, shear banding becomes increasingly more difficult to initiate. Correspondingly, the strength and achievable elastic strain rise to about twice those of bulk samples of this MG. This size regime is modeled to exhibit an obvious size dependence, which can be represented by a shifted-$D^{-0.5}$ power law. The accumulative data sets for several MG in the literature appear to support such a general trend. The combination of unprecedented high strength and high elastic strain limit renders small-volume MG very attractive for practical use in devices and microsystems.

Acknowledgements

This work was supported by NSFC (50925104), the 973 Programs of China (2010CB631003, 2012CB619402) and adjunct professorship at XJTU (E.M., J.L.). J.L. also acknowledges support by NSF DMR-1008104 and DMR-1120901, and AFOSR FA9550-08-1-0325. E.M., J.D. and Y.Q. C. were supported at JHU by US-NSF-DMR-0904188.

Appendix A. Supplementary material

Supplementary data associated with this article can be found, in the online version, at http://dx.doi.org/10.1016/j.actamat.2012.06.019.

References

[1] Greer AL, Ma E. MRS Bull 2007;32:611.
[2] Schuh CA, Hufnagel TC, Ramamurty U. Acta Mater 2007;55:4067.
[3] Kumar G, Tang HX, Schroers J. Nature 2009;457:868.
[4] Guo H, Yan PF, Wang YB, Tan J, Zhang ZF, Sui ML, et al. Nat Mater 2007;6:735.
[5] Volkert CA, Donohue A, Spaepen F. J Appl Phys 2008;103:6.
[6] Jang DC, Greer JR. Nat Mater 2010;9:215.
[7] Deng QS, Cheng YQ, Yue YH, Zhang L, Zhang Z, Han XD, et al. Acta Mater 2011;59:6511.
[8] Yavari AR, Georgarakis K, Botta WJ, Inoue A, Vaughan G. Phys Rev B 2010;82:172202.
[9] Shan ZW, Li J, Cheng YQ, Minor AM, Asif SAS, Warren OL, et al. Phys Rev B 2008;77:6.
[10] Chen CQ, Pei YT, De Hosson JTM. Acta Mater 2010;58:189.
[11] Bharathula A, Lee SW, Wright WJ, Flores KM. Acta Mater 2010;58:5789.
[12] Yang Y, Ye JC, Lu J, Gao YF, Liaw PK. JOM 2010;62:93.
[13] Kumar G, Desai A, Schroers J. Adv Mater 2011;23:461.
[14] Uchic MD, Dimiduk DM, Florando JN, Nix WD. Science 2004;305:986.
[15] Greer JR, De Hosson JTM. Prog Mater Sci 2011;56:654.
[16] Greer JR, Oliver WC, Nix WD. Acta Mater 2005;53:1821.
[17] Dimiduk DM, Uchic MD, Parthasarathy TA. Acta Mater 2005;53:4065.
[18] Zhu T, Li J. Prog Mater Sci 2010;55:710.
[19] Schuster BE, Wei Q, Hufnagel TC, Ramesh KT. Acta Mater 2008;56:5091.
[20] Jang DC, Gross CT, Greer JR. Int J Plast 2011;27:858.
[21] Yang Y, Ye JC, Lu J, Wang Q, Liaw PK. J Mater Res 2010;25:563.
[22] Wu XL, Guo YZ, Wei Q, Wang WH. Acta Mater 2009;57:3562.
[23] Bharathula A, Flores KM. Acta Mater 2011;59:7199.
[24] Lai YH, Lee CJ, Cheng YT, Chou HS, Chen HM, Du XH, et al. Scripta Mater 2008;58:890.
[25] Dubach A, Raghavan R, Loffler JF, Michler J, Ramamurty U. Scripta Mater 2009;60:567.
[26] Ye JC, Lu J, Yang Y, Liaw PK. Intermetallics 2010;18:385.
[27] Lee CJ, Huang JC, Nieh TG. Appl Phys Lett 2007;91:161913.
[28] Kuzmin OV, Pei YT, Chen CQ, De Hosson JTM. Acta Mater 2012;60:889.
[29] Shi YF. Appl Phys Lett 2010;96:121909.
[30] Tian L, Cheng YQ, Shan ZW, Li J, Wang CC, Han XD, et al. Nat Commun 2012;3:609.
[31] Shan ZW, Mishra RK, Asif SAS, Warren OL, Minor AM. Nat Mater 2008;7:115.
[32] Yang BJ, Yao JH, Zhang J, Yang HW, Wang JQ, Ma E. Scripta Mater 2009;61:423.
[33] Inoue A. Prog Mater Sci 1998;43:365.
[34] Zheng K, Wang CC, Cheng YQ, Yue YH, Han XD, Zhang Z, et al. Nat Commun 2010;1:24.
[35] Yang Y, Ye JC, Lu J, Liu FX, Liaw PK. Acta Mater 2009;57:1613.
[36] Ye JC, Lu J, Yang Y, Liaw PK. Acta Mater 2009;57:6037.
[37] Cheng YQ, Ma E. Prog Mater Sci 2011;56:379.
[38] Johnson WL, Samwer K. Phys Rev Lett 2005;95:195501.
[39] Shimizu F, Ogata S, Li J. Acta Mater 2006;54:4293.
[40] Han Z, Tang LC, Xu J, Li Y. Scripta Mater 2009;61:923.
[41] Cheng YQ, Ma E. Acta Mater 2011;59:1800.
[42] Falk ML, Langer JS. Phys Rev E 1998;57:7192.
[43] Sevillano JG, Arizcorreta IO, Kubin LP. Mater Sci Eng A – Struct Mater Prop Microstruct Process 2001;309:393.
[44] Chen C, Pei Y, Kuzmin O, Zhang Z, Ma E, De Hosson J. Phys Rev B 2011;83:180201.
[45] Jiang WH, Atzmon M. Acta Mater 2003;51:4095.
[46] Klaumünzer D, Lazarev A, Maaß R, Dalla Torre F, Vinogradov A, Löffler J. Phys Rev Lett 2011;107:185502.
[47] Klaumuenzer D, Maass R, Loeffler JF. J Mater Res 2011;26:1453.
[48] Yang Y, Ye JC, Lu J, Liu CT. Intermetallics 2011;19:1005.
[49] Yang Y, Ye JC, Lu J, Liaw PK, Liu CT. Appl Phys Lett 2010;96:011905.